hydrogen

MDPI

Article

Characterization and Thermochemical Conversion of Mixed Plastic Waste (Plasmix) Through Pyrolysis and Hydrogasification

Maria Beatrice Falasconi [1,2], Sara Tatarelli [1], Lorenzo De Paola [1,3], Giampaolo Caputo [3], Pietro Colucci [3], Fabio Codignole Luz [3], Vincenzo Piemonte [1], Giulia Monteleone [3] and Alberto Giaconia [3,*]

1 Unit of Chemical-Physics Fundamentals in Chemical Engineering, Department of Science and Technology for Sustainable Development and One Health, University Campus Bio-Medico of Rome, Via Alvaro Del Portillo, 21, 00128 Rome, Italy
2 High Temperature Processes Unit, Instituto Madrileño de Estudios Avanzados Energy, Avda. Ramón de la Sagra, 3, 28935 Móstoles, Spain
3 Laboratory for Hydrogen and New Energy Vectors, Department of Energy Technologies and Renewable Sources, ENEA Casaccia Research Center, Via Anguillarese, 301, 00123 Rome, Italy
* Correspondence: alberto.giaconia@enea.it

Abstract

The thermochemical valorization of non-recyclable mixed plastic waste represents a promising strategy for waste management and energy recovery. This work experimentally investigates the hydrogasification of Plasmix, the residual fraction of mixed plastic waste not mechanically recyclable, and compares it with conventional pyrolysis at 550 °C and 2.1 bar. Hydrogasification of low-density polyethylene (LDPE) was also investigated to assess the influence of feedstock composition. Feedstocks were characterized by elemental, proximate, and thermal analyses, while product distribution, methane evolution, and condensable products were evaluated by online gas analysis and gas chromatography–mass spectrometry. For Plasmix, hydrogasification increased the gas yield from 53.1% during pyrolysis to 74.0% and methane yield from 4.2 to 13.3%, while reducing the liquid fraction from 29.6 to 14.4%. Methane evolution indicated a two-stage mechanism involving initial devolatilization followed by hydrogen-assisted conversion of residual carbonaceous species. LDPE hydrogasification achieved a gas yield of 85.3% and nearly complete feedstock conversion. These results demonstrate that hydrogasification promotes methane-rich gas production from mixed plastic waste under relatively mild operating conditions, providing a basis for integration with innovative steam methane reforming units, potentially allowing the hydrogen required for hydrogasification to be internally generated while achieving net hydrogen production.

Keywords: hydrogasification; waste-to-fuel; plasmix; mixed plastic waste valorization; pyrolysis; methane production; hydrogen; thermochemical recycling

Check for updates

Academic Editor: Isabel Cabrita

Received: 31 August 2026
Revised: 29 October 2026
Accepted: 31 October 2026
Published: 5 November 2026

Copyright: © 2026 by the authors. Licensee MDPI, Basel, Switzerland. This article is an open access article distributed under the terms and conditions of the Creative Commons Attribution (CC BY) license.

1. Introduction

Rapid economic growth and improved living standards have accelerated the depletion of conventional fossil fuel reserves, whose extensive exploitation has significantly contributed to environmental pollution. Concurrently, global energy demand continues to rise, primarily driven by population growth [1]. This scenario highlights the urgent need to develop sustainable energy alternatives to reduce greenhouse gas emissions and meet increasing energy requirements. Despite technological advances, renewable energy sources often face economic challenges that limit their large-scale deployment, making

their widespread adoption dependent on supportive policies and transition frameworks [2]. Within this context, carbon-based materials and biomass, including agricultural and industrial residues, woody biomass, municipal solid waste, and plastic wastes, emerge as promising candidates for energy generation. These feedstocks provide a double benefit such as energy recovery and waste volume reduction, contributing simultaneously to energy security and environmental sustainability [3]. In 2022, the European production of plastics reached 58.8 Mt, of which 80.3% was fossil-based and only 19.7% circular (mechanically recycled, chemically recycled, or bio-based). Polypropylene (PP) and polyethylene (PE) represented about 37% of total production. Of the 32.3 Mt of collected post-consumer plastic wastes, 26.9% was recycled, 49.6% was used for energy recovery, and 23.5% was landfilled. Although recycling rates have improved, the still low recycling fraction poses a major challenge for waste management. Consequently, European governments are focusing on improving collection and conversion technologies to achieve a "zero landfilling" scenario by 2050 [4]. Plastic wastes can be managed through four main routes: mechanical recycling, biological recycling (for biodegradable polymers), chemical recycling, and energy recovery via incineration [5]. Among these, chemical recycling (e.g., pyrolysis, gasification and hydrogasification) is particularly suitable for mixed or contaminated plastics that are hard to separate. This approach allows simultaneous processing of different polymer types with a higher tolerance to impurities [6], making it especially advantageous for complex waste streams such as Plasmix, the non-recyclable fraction from mechanical recycling plants. Plasmix is a heterogeneous mixture primarily composed of polyolefins (PE and PP), with minor amounts of PET, PS, PVC, and non-plastic contaminants such as paper, textiles, metals and inert residues [7]. It retains an energy potential comparable to certain fossil fuels, such as coke, but owing to its mixed and contaminated nature, it cannot be efficiently recycled through conventional mechanical processes and is therefore mostly destined for incineration, co-processing in cement kilns, or landfilling [8,9].

Unlike O_2/air gasification, hydrogasification operates in a reducing atmosphere, converting the carbonaceous feedstock (including wet and chlorinated wastes) in a syngas composed mainly of methane through an exothermic process involving external hydrogen input. This reducing environment minimizes the formation of toxic compounds (e.g., dioxins, furans) and promotes methane formation [10], as described by the following global reaction (Equation (1)):

$$C_xH_yO_{z(s)} + (2x + z - 0.5y)H_{2(g)} \rightarrow xCH_4 + zH_2O_{(g)} \quad (1)$$

In reality, hydrogasification is a complex reactive system, where the dominant reactions depend on temperature, residence time, and the feedstock's chemical composition [11]. The process involves a combination of pyrolysis, hydrogenation, reforming, and water–gas shift reactions [12] whose equilibrium strongly influences the final distribution of gaseous, liquid, and solid products. The process generally occurs in two main stages [13–16]: an endothermic pyrolysis step, in which solid polymers decompose into volatiles and char, producing condensable products (oils and tar) and light gases (C_1–C_4 hydrocarbons, CO, CO_2, and H_2), followed by an exothermic hydrogenation stage, where the pyrolysis intermediates react with H_2 to form CH_4 and other saturated hydrocarbons [17–19].

In a recent study, Giaconia et al. [20] demonstrated the potential to integrate hydrogasification with steam methane reforming (SRM) to establish a circular hydrogen production loop, where the CH_4 produced in hydrogasification is reformed to generate additional hydrogen. Part of this hydrogen can be recycled to feed the hydrogasification reactor, while the surplus constitutes net hydrogen production for external use.

In this framework, the present study investigates the thermochemical conversion of typical Plasmix wastes, supplied by a municipal recycling consortium, through pyrolysis and

hydrogasification. The aim is to evaluate the influence of hydrogen on product distribution and gas composition. Moreover, a comparison between Plasmix and LDPE hydrogasification is carried out to assess the effect of feedstock heterogeneity on process performance. Among gaseous products, methane has a key role in the potential integration of hydrogasification with steam methane reforming (SRM) for the development of sustainable and circular waste-to-hydrogen energy systems.

2. Material and Methods

2.1. Preparation of the Plastic Solid Waste Samples

The Plasmix employed in this study (Figure 1) was supplied by a municipal recycling consortium (Rome, Italy) to the ENEA Casaccia Research Center. For preliminary chemical–physical characterization, samples were washed with distilled pure water to remove possible impurities, then ground using an electric shredder (Power Black Titanium 2500 Max Smart, Cecotec Innovaciones S.L., Alfafar, Valencia, Spain) and sieved with a mechanical shaker to obtain a uniform particle size (<0.5 mm). The prepared material was finally stored in sealed plastic containers for subsequent chemical–physical characterization (Section 2.2). In the case of the hydrogasification and pyrolysis tests (Section 2.3), Plasmix was used as received from the supplier, without pre-treatment, in order to preserve the original heterogeneity of the waste stream and reproduce conditions closer to realistic industrial applications.



Figure 1. Plasmix sample used in this work.

2.2. Characterization of Plastic Solid Wastes

Chemical–physical characteristics of Plasmix sample were determined by proximate analysis, ultimate analysis, carbon fraction analysis (TOC/ROC/TIC) and heating value determination (HHV and LHV). Each analysis was repeated at least three times, and the characterization results were expressed in terms of averages.

2.2.1. Proximate Analysis

Proximate analysis (moisture, volatile matter, fixed carbon, and ash content) was performed on ≈10 mg sample in open 30 µL alumina crucibles using a Mettler Toledo TGA/DSC1 analyzer (Mettler-Toledo GmbH, Greifensee, Switzerland), controlled by STARe software (V19.0). Blank runs corrected for buoyancy effects. The thermal program used N_2 carrier gas at 60 mL min^{-1}, with 90 mL min^{-1} air introduced in step 5:

1. 25 °C isotherm (5 min)
2. Heating at 20 °C min^{-1} to 105 °C
3. 105 °C isotherm (15 min)—Moisture loss (steps 1–3)

4. Heating at 20 °C min^{-1} to 900 °C—Volatile matter release
5. 900 °C isotherm (5 min, N_2/air)—Char combustion (mass loss) and Ash content (residual weight).

2.2.2. Ultimate Analysis

Elemental composition (C, H, N, and S) was determined using a LECO TruSpec® analyzer (LECO Corporation, St. Joseph, MI, USA) by high-temperature combustion of ~2 mg samples, followed by gas detection via infrared (IR) and thermal conductivity detectors (TCD), with oxygen content calculated by difference. Calibration was performed using certified reference materials to ensure measurement reliability, accuracy, and reproducibility.

2.2.3. Carbon Fraction Analysis

The carbon speciation of the Plasmix feedstock was determined using an Elementar soli TOC cube analyzer (Elementar Analysensysteme GmbH, Langenselbold, Germany), which quantifies total organic carbon (TOC), residual oxidizable carbon (ROC), and total inorganic carbon (TIC) according to the DIN 19539 standard [21]. A temperature ramping program up to 900 °C with a rate of 50 °C min^{-1} is applied to a sample of approximately 50 mg: TOC is determined at 400 °C, ROC between 400 °C and 600 °C and TIC between 600 °C and 900 °C. Nitrogen and oxygen were used as carrier and oxidizing gases, respectively. The CO_2 evolved at the different temperature stages is quantified by an IR detector, representing the various carbon fractions.

2.2.4. Heating Values Calculation

The higher heating value (HHV) on a dry basis was estimated using the Dulong–Berthelot correlation, expressed as shown in Equation (2) [22].

$$HHV(\mathrm{MJ/kg}) = 0.3414{\cdot}C(\%) + 1.4445{\cdot}H(\%) - \frac{N(\%) + O(\%) - 1}{8} + 0.093{\cdot}S(\%) \quad (2)$$

The lower heating value (LHV) on a dry basis was determined using Equation (3), which subtracts the latent heat of water vaporization from the HHV [23].

$$LHV(\mathrm{MJ/kg}) = HHV(\mathrm{MJ/kg}) - 0.2183 \cdot H(\%) \quad (3)$$

2.2.5. Thermal Degradation Analysis

The pyrolysis of polymers involves the scission of macromolecular chains, leading to the formation of volatile species and a progressive mass loss of the material. Consequently, thermal degradation tests have been carried out to provide comprehensive information on the thermal stability and degradation behaviour of the material, conducting thermogravimetric analysis (TGA) and Differential Scanning Calorimetry (DSC) analysis [24]. Each test was performed using a sample mass of approximately 10 mg, placed in a 30 µL alumina crucible. Nitrogen was used as the carrier gas at a flow rate of 100 mL min^{-1}. TGA of Plasmix samples was conducted using a Mettler Toledo TGA/DSC1 thermogravimetric analyzer (Mettler-Toledo GmbH, Greifensee, Switzerland) following a specific temperature program consisted of a single heating ramp from 20 °C to 1000 °C at a rate of 10 °C min^{-1}. The weight loss and derivative weight loss were evaluated for each sample, and the maximum degradation temperature was determined in correspondence of the maximum decomposition rate. The K–K method, developed by Li et al. [25,26], was employed to identify the decomposition peaks of the main species present in the Plasmix samples. DSC analysis was performed using a HITACHI NEXTA STA300 (TG–DTA mode) instrument (Hitachi High-Tech Corporation, Tokyo, Japan)to identify characteristic endothermic and

exothermic events, evaluating the thermal transitions of the Plasmix sample, such as melting and degradation reactions.

2.3. Experimental Set-Up and Conditions of the Hydrogasification and Pyrolysis Tests

The experimental set-up employed for the hydrogasification and pyrolysis tests consists of three main sections, as schematically reported in Figure 2. The final configuration was progressively optimized through preliminary experimental campaigns aimed at improving gas flow stability, product collection, pressure control, and analytical reliability.

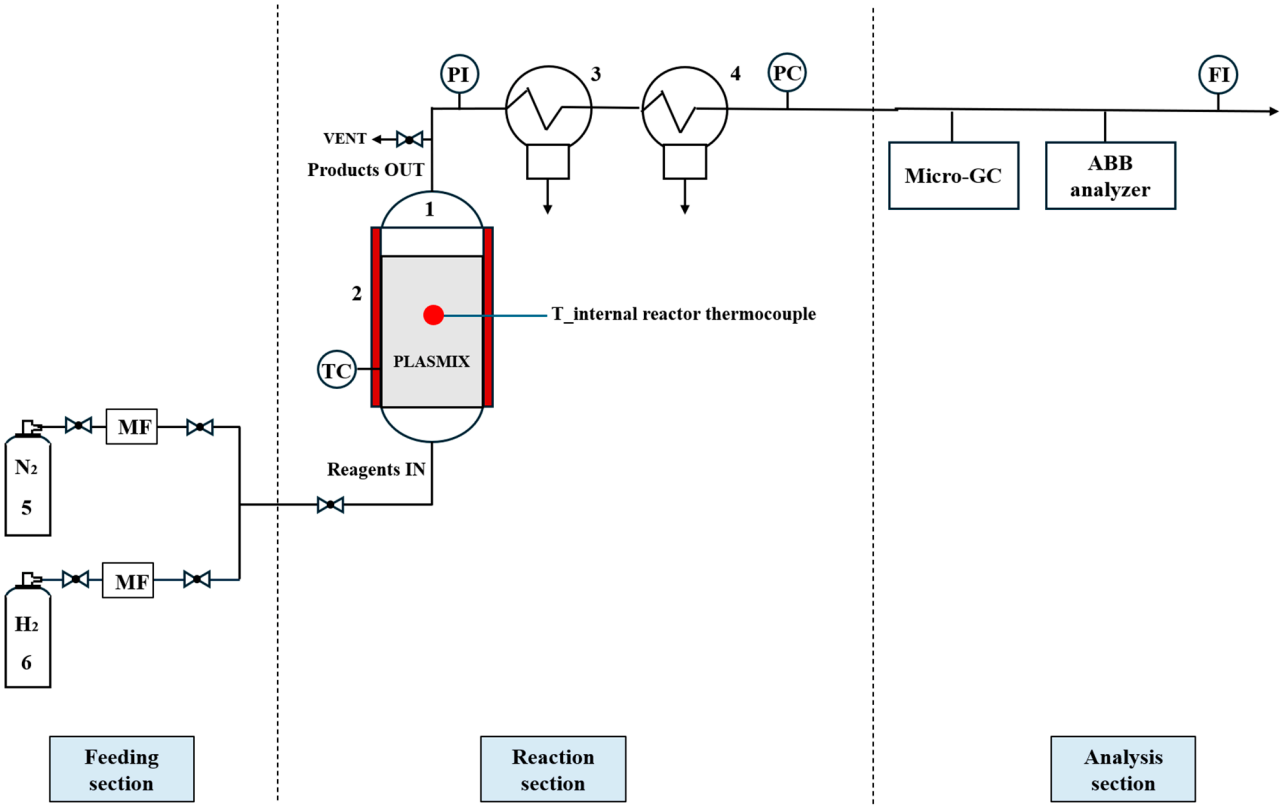

Figure 2. Scheme of the experimental setup: (1) semi-batch reactor; (2) electric heater; (3) primary condenser; (4) secondary condenser; (5) nitrogen cylinder; (6) hydrogen cylinder.

The feeding section is equipped with mass flow controllers (MFCs) used to regulate the inlet gas streams. Hydrogen (H_2) was supplied as reactive gas during hydrogasification tests, while nitrogen (N_2) was used both as inert carrier gas and internal tracer for the determination of the total outlet gas flow rate. The total molar gas flow rate exiting the reactor (F_{tot}^{out} expressed in mol·min^{-1}) was calculated through the nitrogen mass balance according to Equation (4):

$$F_{tot}^{out} \cdot = \frac{F_{tot}^{in} \cdot X_{N2}^{in}}{X_{N2}^{out}} \quad (4)$$

where F_{tot}^{in} (mol·min^{-1}) is the total molar flow rate of the feed gas, while X_{N2}^{in} and X_{N2}^{out} are the nitrogen molar fractions at the reactor inlet and outlet, respectively.

The reaction section consists of a stainless-steel reactor operated in a batch-solid/semi-continuous-gas configuration, with the solid feedstock loaded prior to each experiment and, N_2 and, eventually, H_2 continuously supplied. The reactor has an internal diameter of 5 cm, a height of 18.5 cm, and is externally heated by electrical resistance bands. The gaseous products exiting the reactor pass through two condensers maintained at −2 °C to collect water, condensable hydrocarbons and minimize tar accumulation along the downstream

lines. Reactor temperature was monitored by a K-type thermocouple positioned at the reactor center. A pressure controller installed downstream of the condensers maintained the reactor pressure at 2.1 bar during all experiments. This pressure was selected as a laboratory screening condition to ensure stable gas sampling and proper operation of the Micro GC, rather than as an optimized process-design condition.

The analytical section consists of a Varian CP-4900 Micro Gas Chromatograph (Micro GC; Varian B.V., Middelburg, The Netherlands) and an ABB AO2020 continuous gas analyzer (ABB Automation GmbH, Frankfurt am Main, Germany) operating in parallel for real-time gas composition measurements. Calibration was performed using certified gas mixtures containing known concentrations of H_2, N_2, oxygen (O_2), carbon monoxide (CO), carbon dioxide (CO_2), and methane (CH_4).

Hydrogasification and pyrolysis experiments were conducted following the same optimized operating procedure using either Plasmix or pure LDPE as feedstock. Plasmix was used as received from the supplier, without pre-treatment, in order to preserve the original heterogeneity of the waste stream and reproduce conditions closer to realistic industrial applications. For each experiment, 25 g of feedstock was loaded at room temperature into the reactor filling the entire available volume, which was subsequently sealed and purged with nitrogen to remove residual air. The reactor was then heated from room temperature to 550 °C at a constant heating rate of 20 °C·min^{-1} while maintaining the operating pressure at 2.1 bar.

The operating temperature of 550 °C was selected based on preliminary tests, which showed an increase in methane production and hydrogen conversion at higher temperatures, indicating kinetically controlled hydrogasification reactions. At the same time, this temperature remains relatively low compared to conventional thermochemical recycling processes, improving the potential energetic competitiveness of the process while keeping the system below the hydrogen auto-ignition temperature for safety reasons.

Regarding the operating pressure, the slight overpressure was selected to ensure stable sampling conditions and proper aspiration by the Micro GC during continuous gas analysis.

During hydrogasification tests, hydrogen and nitrogen were fed at flow rates of 100 NmL·min^{-1} and 15 NmL·min^{-1}, respectively. Pyrolysis tests were instead carried out under a pure nitrogen flow of 115 NmL·min^{-1} to ensure inert conditions while maintaining the same total inlet gas flow rate. The selected hydrogen flow rate was chosen to increase hydrogen residence time inside the reactor; indeed, preliminary experiments performed at higher hydrogen flow rates (200 NmL·min^{-1}) resulted in lower methane formation probably due to insufficient residence time of the produced gas mixture in the reactor.

Gas composition and flow rates were continuously monitored throughout the experiments.

At the end of each test, condensable products collected in the cold traps were weighed, diluted in n-hexane, and centrifuged at 10,000 rpm for 10 min to remove possible suspended solids. The resulting liquid phase was analyzed by gas chromatography–mass spectrometry (GC-MS, Thermo Scientific TRACE GC, Thermo Fisher Scientific, Rodano, Milan, Italy) for condensable product characterization.

After cooling the reactor under N_2, the residual solid products were recovered and weighed. The measured masses of the liquid and solid products were used to evaluate the overall mass balance and product yields. Gas yields were calculated by closing the mass balance since only the total molar flow rate of the gas was monitored, and only the main product compounds had their mass flow rates monitored.

Table 1 summarizes the main operating conditions adopted for hydrogasification and pyrolysis experiments.

Table 1. Operative conditions in the experimental tests.

Parameter	Hydrogasification Conditions	Pyrolysis Conditions
Waste input	25 g	25 g
Input gas flow rate	100 Nml·min^{-1} H_2 15 Nml·min^{-1} N_2	115 Nml·min^{-1} N_2
Reactor temperature	550 °C	550 °C
Heating ramp	20 °C·min^{-1}	20 °C·min^{-1}
Pressure	2.1 bar	2.1 bar
Condensation temperature	−2 °C	−2 °C

3. Results

3.1. Chemical–Physical Characterization of Plastic Solid Wastes

Table 2 shows the results for proximate analysis, ultimate analysis, carbon fraction analysis (TOC/ROC/TIC) and the heating values of the Plasmix samples.

Table 2. Results for Proximate analysis, ultimate analysis, carbon fraction analysis and heating values of the Plasmix samples.

Proximate analysis	
Moisture (as-received basis) (%)	0.11
Volatile matter (VM) (dry basis) (%)	94.95
Fixed carbon (FC) (dry basis) (%)	2.94
Ash (dry basis) (%)	2.11
Elemental analysis (dry basis)	
Carbon (C) (%)	82.39
TOC (%)	77.31
ROC (%)	3.83
TIC (%)	1.25
Hydrogen (H) (%)	12.83
Nitrogen (N) (%)	0.18
Sulfur (S) (%)	-
Oxygen (O) (%)	2.49
Heating value	
HHV (MJ/kg)	46.45
LHV (MJ/kg)	43.65

A high volatile matter content (94.95%) was observed, indicating that this waste material is particularly suitable for thermochemical conversion processes. This characteristic promotes the formation of gaseous and liquid products during pyrolysis or hydrogasification. Furthermore, the high HHV and LHV highlight its strong potential for thermochemical

valorization [27]. Composition and characteristics of Plasmix are comparable to those of other mixed plastic waste materials reported in the literature [28–31]. In addition, the ultimate analysis reveals that the percentage of heteroatoms is not significant, indicating that Plasmix has the potential to transform into an excellent fuel. In fact, its low nitrogen (0.18%) and sulfur contents are advantageous, as they limit the formation of harmful gases such as nitrogen oxides (NO_x) and sulfur oxides (SO_x) during thermal conversion. The predominance of organic carbon (TOC = 77.31%) and the low inorganic fraction (TIC = 1.25%) is consistent with the high volatile matter and low ash content, thus indicating a feedstock largely composed of reactive organic species suitable for gas production. It should be noted that, due to the heterogeneous nature of Plasmix and the possible presence of PVC, chlorine-containing compounds such as HCl may also be released during thermal conversion. Their presence and concentration could not be quantitatively determined in the present study and should therefore be considered in the design of downstream gas-cleaning units to protect the reactor and downstream equipment, particularly in view of potential SMR integration.

3.2. Thermal Degradation Results

The thermal characterization of the Plasmix sample reveals a multi-stage degradation process, which is typical of heterogeneous plastic mixtures. Figure 3 shows the results of the thermogravimetric analysis in terms of TG, DTG and DDTG curves within a temperature range up to 1000 °C. Figure 4 combines the TG and DTG curves with the DSC one, but only analyzes the temperature range up to 500 °C.

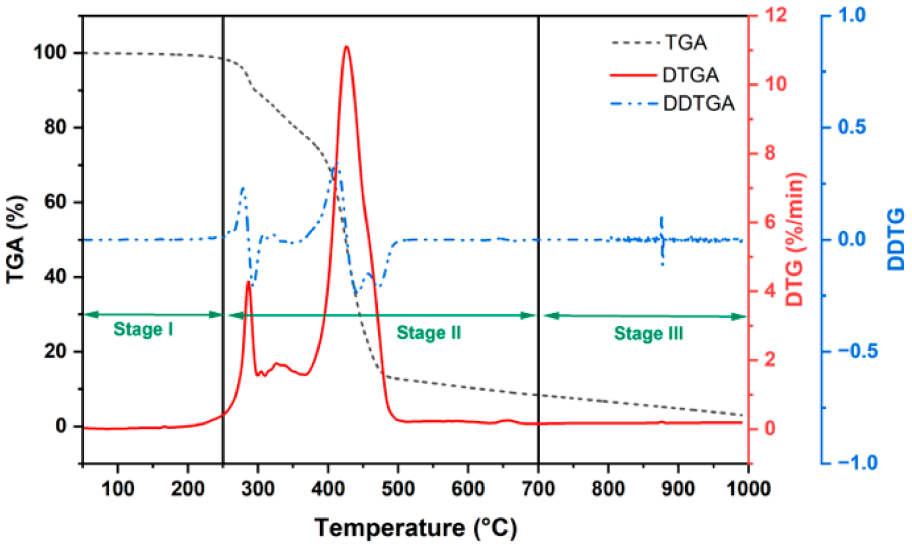

Figure 3. Thermogravimetric analysis (TGA), derivative thermogravimetric analysis (DTG) and second derivative thermogravimetric analysis (DDTG) curves of the Plasmix at 10 °C min^{-1}.

The TGA curve shows that the sample remains almost thermally stable up to approximately 250–270 °C, with only a very limited mass loss in this initial region, corresponding to the loss of moisture and light volatile compounds (<2%) (Stage I in Figure 3). This behavior is consistent with the DSC signal, where a small endothermic peak appears between about 107 and 162 °C. Since no significant mass loss is observed in the TGA in this temperature range, this event can reasonably be attributed to the melting of some thermoplastic fractions rather than to chemical degradation. Specifically, endothermic peaks appear at 107.55 °C, 122.5 °C, and 162.18 °C, corresponding to the melting transitions of LDPE, HDPE, and PP, respectively [32], which are the main components of the heterogeneous Plasmix samples.

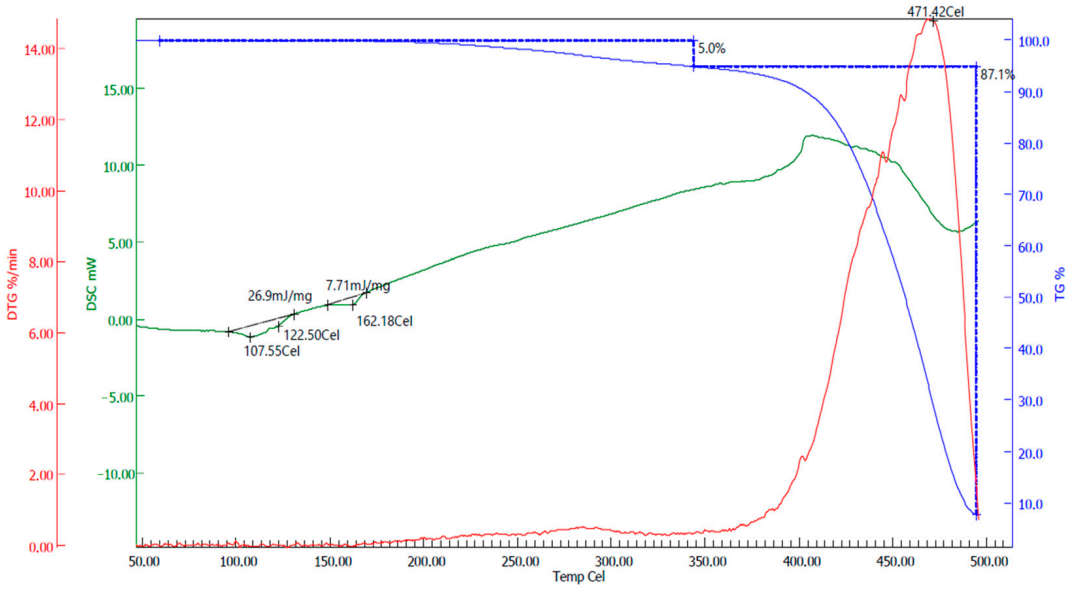

Figure 4. Thermogravimetric (TG), Derivative Thermogravimetric (DTG), and Differential Scanning Calorimetry (DSC) (endo-down) curves of the Plasmix at 10 °C min^{-1}.

The main degradation stage occurs between approximately 250 and 500 °C (Stage II in Figure 3). In this region, initially, above approximately 400 °C, an exothermic contribution becomes evident, likely associated with secondary reactions involving degradation intermediates, such as radical recombination, cyclization, aromatization, and char-forming processes. These processes release heat as polymer fragments recombine and form more stable unsaturated and aromatic structures, preceding the complete volatilization observed in the TGA results. In fact, after that, the TGA curve exhibits the sharpest mass decrease, while the DTG curve reaches its maximum degradation rate around 430–470 °C, with the main DTG peak centered close to 471 °C. This indicates that the majority of the volatile fraction is released in this temperature interval. The DSC curve simultaneously shows an intense endothermic event associated with the decomposition process.

The overlap of these endothermic and exothermic contributions is consistent with the complex composition of Plasmix and confirms that the degradation process does not occur through a single mechanism. The presence of shoulders and smaller DTG contributions before the main peak indicates that degradation does not occur through a single reaction pathway. Instead, different plastic fractions are likely decomposed at different temperatures. This interpretation is confirmed by the DDTG signal in Figure 3, where changes in curvature identify multiple overlapping decomposition phenomena rather than one unique degradation event.

Above approximately 500 °C, the degradation rate rapidly decreases and the sample enters Stage III (Figure 3). The TGA curve approaches a residual mass of about 5%, indicating that most of the organic fraction has been volatilized, according also with the results of the proximate analysis in Table 1. The remaining residue is likely associated with fixed carbonaceous material and inorganic ash components. The absence of further significant DSC or DTG peaks at higher temperatures confirms that the main decomposition reactions are essentially completed below 500 °C.

Overall, the combined TGA/DTG/DDTG and DSC analyses indicate that the Plasmix sample undergoes an initial melting phase followed by a complex multi-step thermal degradation dominated by volatilization reactions between 300 and 500 °C. The very high total mass loss confirms the predominance of volatile organic matter in the sample, while the limited final residue suggests a relatively low ash content.

3.3. Experimental Hydrogasification and Pyrolysis Tests

3.3.1. Products Distribution

Table 3 summarizes the product yields obtained from Plasmix pyrolysis, Plasmix hydrogasification, and LDPE hydrogasification at 550 °C. Each yield is expressed as mass yield and referred to the initial mass of solids loaded into the reactor. The results clearly show that the presence of hydrogen strongly promotes the conversion of the solid feedstock into volatile products compared to conventional pyrolysis. In particular, the overall volatile product yield, calculated as the sum of gaseous and liquid products, increased from 82.73% during Plasmix pyrolysis to 88.44% during hydrogasification. This trend is quite consistent with the high volatile matter content measured during proximate analysis (94.95%, Section 3.1) and confirms that hydrogen enhances feedstock conversion while limiting secondary char formation. The highest volatile product yield was obtained during LDPE hydrogasification (99.40%), in agreement with the simpler chemical structure of polyethylene and the absence of inorganic impurities.

Table 3. Summary of product yields for Plasmix pyrolysis and hydrogasification and LDPE hydrogasification.

T (°C)	Process	Solid Products (w/w %)		Liquid Products (w/w %)	Gaseous Products (w/w %)	Main Gaseous Products		
		Char	Ash			CH_4 (w/w %)	CO_2 (w/w %)	CO (w/w %)
550	Hydrogasification of Plasmix	11.56		14.43	74.01	13.29	5.53	1.37
		8.39	3.17					
	Pyrolysis of Plasmix	17.28		29.59	53.14	4.18	3.75	0.71
		11.83	5.44					
	Hydrogasification of LDPE	0.6		14.10	85.30	15.02	0.56	0.12
		0.6	-					

A more detailed analysis of the product distribution highlights that hydrogasification strongly promotes the formation of gaseous products: gaseous product yield increased from 53.14% during Plasmix pyrolysis to 74.01% during hydrogasification, while the methane yield increased significantly from 4.18% to 13.29%. At the same time, the liquid fraction decreased from 29.59% to 14.43%. These results indicate that hydrogen promotes the conversion of condensable hydrocarbons into lighter gaseous compounds through secondary cracking, hydrogenation, and reforming reactions. Similar behaviors have been widely reported in the literature for hydrogen-assisted thermochemical conversion processes, where hydrogen enhances tar reforming and methane formation while reducing heavy hydrocarbon fractions [33,34]. The increase in methane production observed during hydrogasification is therefore consistent with the promotion of methanation pathways under hydrogen-rich conditions. Moreover, the higher formation of CO_2 and CO compared to pyrolysis suggests that secondary reforming and oxygen-removal reactions also occur during the process.

The solid residue (Figure 5a) simultaneously decreased from 17.28% during pyrolysis to 11.56% during hydrogasification, indicating a higher overall carbon conversion in the presence of hydrogen. A more detailed analysis of the solid fraction reveals that both the char and ash contents decrease during hydrogasification. In particular, the char fraction decreases from 11.83% during pyrolysis to 8.39% during hydrogasification, suggesting that hydrogen promotes the conversion of carbonaceous residues through secondary gasification

and methanation reactions. The ash fraction (Figure 5b) also decreases from 5.44% to 3.17%. Since ash corresponds to the inorganic non-convertible fraction of the feedstock, this reduction is likely associated with the heterogeneous composition of the Plasmix samples and possible differences in the distribution of inorganic impurities among the tested batches rather than to a real conversion of ash-forming species.



(**a**) (**b**)

Figure 5. Total solid residue (**a**) and ashes (**b**) typically obtained at the end of a hydrogasification test of Plasmix.

The residual solid fraction obtained during pyrolysis is significantly higher than the fixed carbon and ash content measured during proximate and thermogravimetric analyses (Sections 3.1 and 3.2, respectively), where the residual fraction accounted for approximately 5% of the initial feedstock. This discrepancy can be attributed to the different experimental scales and operating conditions. In thermogravimetric analyses, the very small sample mass and optimized heat transfer conditions favor almost complete devolatilization, whereas the larger feedstock amount employed in the semi-batch reactor may promote thermal gradients, incomplete volatilization, and secondary char-forming reactions due to the prolonged residence time of heavy intermediates inside the hot reaction zone. Moreover, thermogravimetric analyses were conducted up to 1000 °C, whereas thermochemical conversion experiments were performed at 550 °C. As can be observed in Figure 3, the TGA shows that the residual mass at 550 °C is more than 10%, which is closer to the value obtained experimentally in the reactor.

The hydrogasification of LDPE resulted in the highest gaseous product yield (85.30%) together with an almost complete conversion of the solid feedstock, leaving only 0.60% of solid residue, entirely composed of char, while no ash formation was detected. Moreover, the concentrations of CO and CO_2 remained below 1%, confirming the negligible oxygen content of polyethylene. Compared to Plasmix, LDPE showed a higher methane yield and lower solid residue formation, indicating a more efficient and selective conversion toward gaseous hydrocarbons. This behavior can be attributed to the simpler chemical structure of polyethylene, which consists almost entirely of linear hydrocarbon chains without significant inorganic impurities or oxygenated compounds. In contrast, the heterogeneous composition of Plasmix, including additives, fillers, multilayer residues, and minor oxygenated fractions, promotes the formation of char and secondary by-products, resulting in a more complex reaction network and lower overall conversion efficiency [35].

Table 4 compares the hydrogasification and pyrolysis processes in terms of the distribution of quantified carbon among gas products. Assuming that the carbon content measured during feedstock characterization (82.39%) is representative of the Plasmix used in the reactor tests, the carbon recovered as CH_4, CO_2 and CO increased from 5.42% of the initial feed carbon during pyrolysis to 14.64% during hydrogasification. This fraction

refers only to the carbon contained in the quantified C-containing gases and should not be interpreted as an overall carbon conversion, since carbon in the solid residue, condensable products, and unquantified C_2–C_4 hydrocarbons is not included. Moreover, the fraction of quantified gas-phase C recovered as methane increased from 70.3% to 82.6%. These results indicate that the hydrogen atmosphere not only enhances gaseous product formation but also affects carbon distribution toward CH_4. The hydrogen contained in methane increased from 0.261 to 0.831 g per 25 g of feedstock; however, this value should not be interpreted directly as hydrogen conversion, because part of the hydrogen contained in CH_4 originates from the feedstock itself, while H_2 may also be produced during the pyrolysis step. The net H_2 consumption was therefore quantified through a global balance of the integrated inlet and outlet H_2 flows, as reported in Table 5. The resulting net H_2 consumption was 0.30 g for Plasmix and 0.35 g for LDPE, corresponding to 13.3% and 10.8% of the total H_2 supplied to the reactor, respectively. These values represent the overall net H_2 consumption and cannot be quantitatively attributed to individual H_2-consuming pathways, such as hydrogenation of pyrolysis intermediates and hydrogasification of the residual carbonaceous fraction. Nevertheless, the positive net H_2 consumption observed for both feedstocks confirms that H_2 actively participates in the reactions occurring under hydrogasification conditions, consistent with the enhanced formation and selectivity toward CH_4 observed for Plasmix.

Table 4. Distribution of quantified carbon among CH_4, CO_2 and CO during Plasmix pyrolysis and hydrogasification. Estimated carbon in feed assuming that the carbon content measured during feedstock characterization (82.39%) is representative of the Plasmix used in the reactor tests. Quantified C gases include CH_4, CO_2 and CO. The reported C-carbon recovery represents only the fraction of feed carbon recovered in these quantified C-containing gases and does not represent an overall carbon balance.

Parameter	Pyrolysis	Hydrogasification
Estimated carbon in feed (g)	20.60	20.60
Carbon in CH_4 (g)	0.784	2.492
Carbon in CO_2 (g)	0.256	0.377
Carbon in CO (g)	0.076	0.147
Carbon in quantified C gases (g)	1.116	3.016
Quantified C-gas recovery (% of feed C)	5.42	14.64
CH_4-C selectivity within quantified C gases (%)	70.3	82.6
Hydrogen contained in CH_4 (g)	0.261	0.831

Table 5. Global H_2 balance and net H_2 consumption during Plasmix and LDPE hydrogasification.

Feedstock	Experimental Time (min)	H_2 Inlet (g)	H_2 Outlet (g)	Net H_2 Consumption (g)	Net H_2 Consumption (%)
Plasmix	250	2.25	1.95	0.30	13.3
LDPE	360	3.24	2.89	0.35	10.8

3.3.2. Gaseous Product Analysis (Methane)

Figure 6 compares the time-dependent methane production during Plasmix pyrolysis, Plasmix hydrogasification, and LDPE hydrogasification at 550 °C. Significant differences are observed both in the methane production rate and in the temporal evolution of the process.

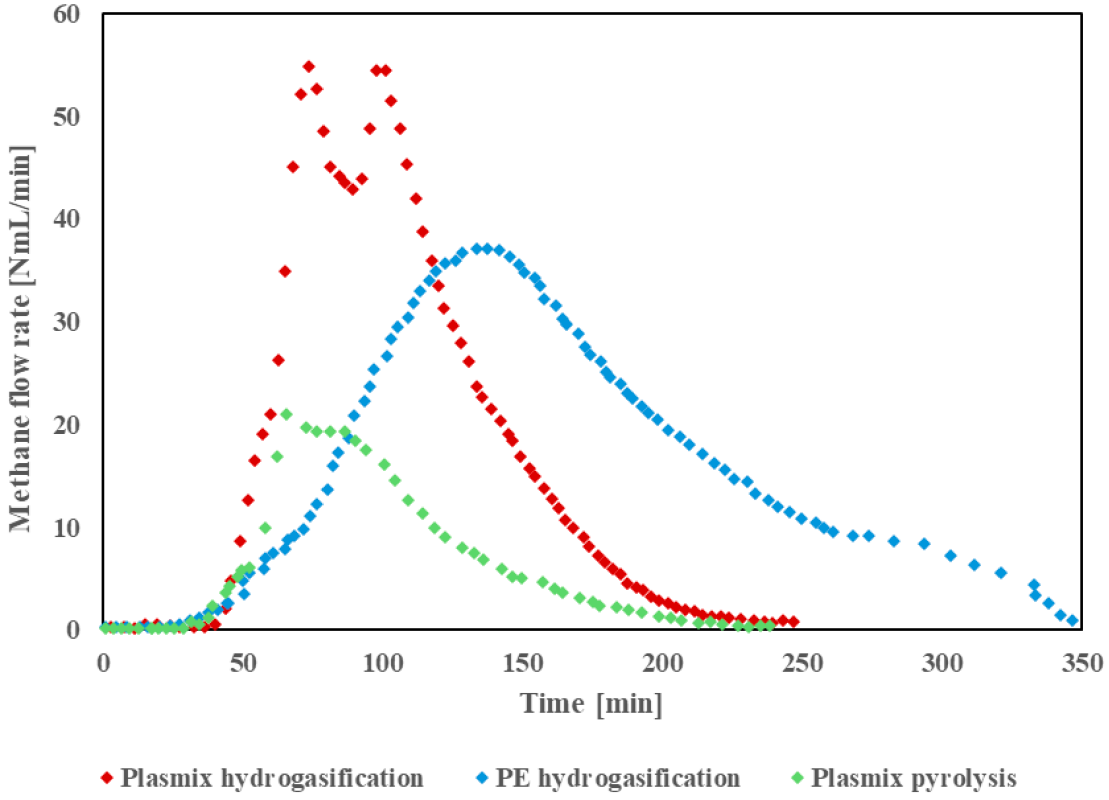

Figure 6. Comparison of methane flow rate (Nml min^{-1}) versus time (min) for Plasmix hydrogasification (red curve), LDPE hydrogasification (blue curve), and Plasmix pyrolysis (green curve).

Compared to pyrolysis, hydrogasification strongly enhances methane formation throughout the reaction. The methane flow rate obtained during Plasmix hydrogasification reaches significantly higher values and exhibits a broader production profile. In both pyrolysis and hydrogasification, an initial methane-production peak is observed in both cases between approximately 60 and 100 min, indicating that the early stage of the process is mainly governed by thermal decomposition and devolatilization of the feedstock. However, under hydrogen atmosphere, methane production remains substantially higher, confirming that hydrogen actively participates in secondary hydrogenation and methanation reactions.

A major difference between the two processes is the appearance of a second methane-production stage during hydrogasification. After the initial devolatilization phase, methane production in pyrolysis rapidly decreases, whereas in hydrogasification methane formation persists for longer periods due to the continued reaction between hydrogen and the heavier carbonaceous residues remaining inside the reactor. This behaviour is consistent with the hypothesis that the molten intermediates and char formed during the first decomposition stage, remaining in the reactor, continue to react under hydrogen atmosphere at 550 °C, promoting additional methane generation. Similar two-stage hydrogasification mechanisms have been reported in the literature [12], where an initial fast pyrolytic decomposition is followed by a slower hydrogen-assisted gasification of the residual char fraction, which exhibits a trigonally bonded structure similar to graphite, as reported by Liu et al. [13] and Tomita et al. [36]. It should be noted that this two-stage interpretation is based on the temporal evolution of the CH_4 flow rate.

The comparison between Plasmix and LDPE hydrogasification further supports this interpretation. In the case of LDPE, methane production occurs over a longer time interval and with a smoother profile, while the second methane-production peak observed for Plasmix is substantially absent. This behaviour is consistent with the almost complete conversion of LDPE into volatile products and the negligible formation of char, as previously

discussed in Section 3.3.1. In contrast, the heterogeneous composition of Plasmix promotes the formation of carbonaceous residues that can undergo secondary hydrogenation reactions at later stages of the process. The broader methane-production profile observed for LDPE may additionally be related to differences in heat transfer and reaction propagation within the molten polymer phase. Conversely, the heterogeneous composition of Plasmix and the possible presence of inorganic impurities or metallic species originating from additives and fillers may promote secondary cracking and hydrogenation reactions, contributing to the earlier methane-production peaks.

This interpretation is further supported by the work of Z. Mısırlıoğlu et al. [37], who reported that the initial rapid stage of hydrogasification corresponds to the conversion of the most reactive or unstable structural sites, such as hydrocarbon side chains and oxygenated groups, followed by a slower stage in which the remaining organic matter is gradually converted into methane. This mechanism is consistent with the longer reaction time observed for LDPE in the present study, since polyethylene is almost entirely oxygen-free and characterized by a more chemically stable structure.

Finally, the enhanced methane formation observed during hydrogasification is also consistent with the product distribution discussed in Table 3, where methane yield increased from 4.18% during pyrolysis to 13.29% during hydrogasification. At the same time, the higher concentrations of CO_2 and CO measured during hydrogasification indicate that reforming and oxygen-removal reactions simultaneously occur in the hydrogen-rich atmosphere.

3.3.3. Liquid Product Analysis

The liquid products collected during the experiments consisted of a viscous dark oil phase (Figure 7), whose yield strongly depended on the operating atmosphere. As previously discussed in Section 3.3.1, the liquid fraction significantly decreased when hydrogen was introduced, dropping from 29.59% during Plasmix pyrolysis to 14.43% during hydrogasification. This behaviour confirms that hydrogen promotes the conversion of condensable hydrocarbons into lighter gaseous products through secondary cracking and hydrogenation reactions.

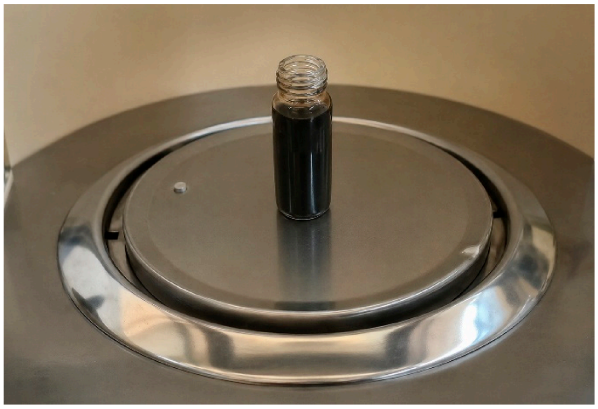

Figure 7. Example of produced oil collected at the end of a hydrogasification test of Plasmix.

The GC-MS analysis of the liquid products is summarized in Figure 8, where the detected compounds are grouped into different chemical families according to carbon number and molecular structure. The complete GC-MS data underlying the grouped compositional analysis are provided in the Supplementary Materials (Table S1 and Figure S1). Most of the identified compounds belong to the C < 13 fraction, which represents the most relevant portion from a fuel-upgrading perspective [38], whereas heavier compounds

correspond mainly to secondary condensation products. The liquid products are predominantly composed of aromatic hydrocarbons, while no significant chlorinated compounds were detected.

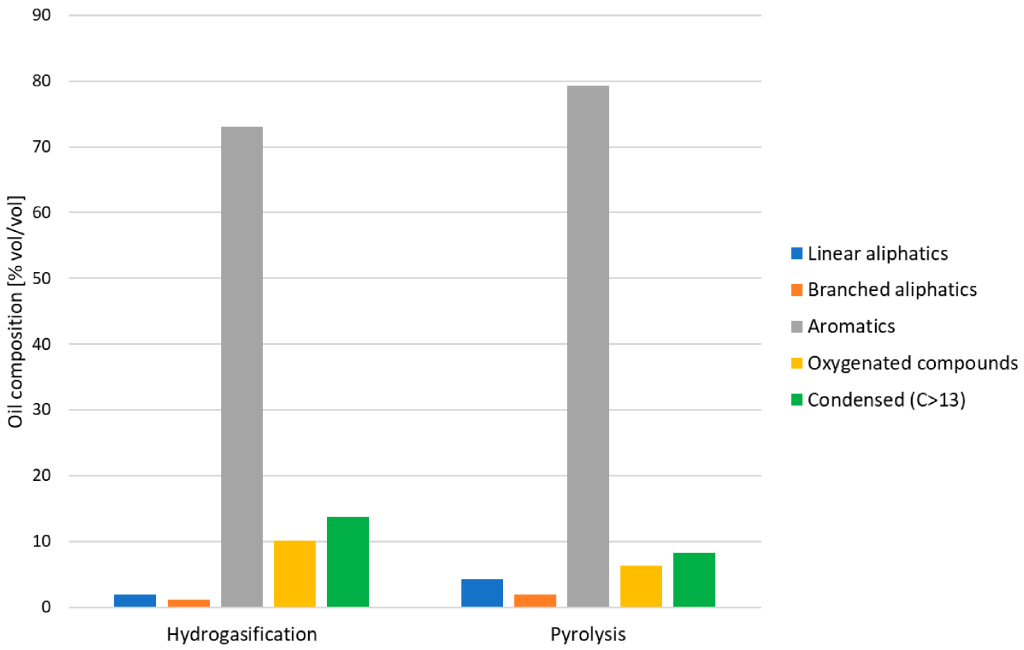

Figure 8. GC-MS analysis of the liquid products collected after hydrogasification and pyrolysis of Plasmix.

Clear differences emerge between pyrolysis and hydrogasification oils. Pyrolysis products exhibit a higher aromatic content [39], consistent with the absence of hydrogenation reactions and with the stronger contribution of thermal cracking and condensation mechanisms. In contrast, hydrogasification promotes the formation of lighter and more saturated compounds while reducing the concentration of oxygenated species [39]. These results are coherent with the simultaneous increase in methane production and reduction in liquid yield observed under hydrogen atmosphere.

The reduction of oxygenated compounds during hydrogasification is additionally consistent with the higher formation of CO and CO_2 reported in Table 3, suggesting that oxygen-removal reactions occur during the conversion process. Overall, the liquid product analysis confirms that hydrogen not only increases the overall volatile product yield but also modifies the chemical nature of the condensable fraction, favouring lighter and less aromatic products compared to conventional pyrolysis.

4. Conclusions

The present work investigated the thermochemical conversion of mixed plastic wastes (Plasmix) through pyrolysis and hydrogasification, with the aim of evaluating the influence of hydrogen on product distribution and methane formation. A comparison with LDPE hydrogasification was additionally carried out to assess the effect of feedstock heterogeneity on process behaviour.

The characterization analyses demonstrated that Plasmix is highly suitable for thermochemical valorization due to its elevated volatile matter content (94.95%) and high heating value (HHV = 46.45 MJ kg^{-1}). Thermal degradation analyses revealed a complex multi-step decomposition mechanism occurring mainly between 250 and 500 °C, associated with the heterogeneous composition of the waste stream.

Experimental results showed that hydrogen strongly modifies the conversion pathways compared to conventional pyrolysis. Under hydrogasification conditions at 550 °C, the gaseous product yield increased from 53.14% to 74.01%, while methane production increased from 4.18% to 13.29%. Simultaneously, the liquid fraction and solid residue decreased significantly, indicating enhanced conversion of condensable hydrocarbons and carbonaceous intermediates through hydrogen-assisted cracking, methanation, and reforming reactions, as confirmed by the literature [33,34].

The time-resolved methane evolution profiles highlighted the presence of a two-stage mechanism during hydrogasification. An initial rapid devolatilization stage was followed by a slower methane-production stage associated with the conversion of residual molten intermediates and char under hydrogen atmosphere. This behaviour was particularly evident for Plasmix and was substantially absent during LDPE hydrogasification, where almost complete conversion into volatile products was achieved with negligible solid residue formation.

Furthermore, hydrogasification significantly reduced the liquid product yield compared to pyrolysis and promoted the formation of lighter and less aromatic condensable compounds. GC-MS analyses showed that the presence of hydrogen favours the formation of lighter compounds and reduces the relative abundance of heavy aromatic species typically associated with conventional pyrolysis oils, which is consistent with the occurrence of secondary cracking and hydrogenation reactions [39]. The comparison between Plasmix and LDPE demonstrated the strong influence of feedstock composition on hydrogasification performance. The simpler and oxygen-free structure of polyethylene promoted higher gas yields and lower char formation, whereas the heterogeneous nature of Plasmix favoured secondary reactions and carbonaceous residue formation.

Overall, the results confirm the potential of hydrogasification as an effective route for the valorization of non-recyclable mixed plastic wastes, enabling enhanced methane production under relatively mild operating conditions. The methane-rich gas obtained could represent a promising intermediate for integration with steam methane reforming processes within circular waste-to-hydrogen systems. Future work should focus on closure of the H_2 mass balance and process optimization through temperature and pressure variation, catalytic hydrogasification, kinetic modelling, and reactor-scale improvements to enhance methane selectivity and overall conversion efficiency. Computational approaches, supported by experimental validation, may further contribute to the optimization of plastic gasification processes and to the investigation of reaction pathways [40]. Furthermore, Raman or FTIR characterization of the residual char could provide additional insights into the structural changes and possible graphitization occurring during hydrogasification. Future studies should also include the quantitative determination of chlorine in the Plasmix feedstock and HCl in the product gas, together with an assessment of their potential implications for downstream gas treatment and SMR catalyst protection.

Supplementary Materials: The following supporting information can be downloaded at: https://www.mdpi.com/article/10.3390/hydrogen7040185/s1, Figure S1: GC–MS data of the individual compounds identified in the liquid products obtained from Plasmix pyrolysis and Plasmix hydrogasification, including their corresponding peak areas and relative peak areas; Table S1: GC–MS data of the individual compounds identified in the liquid products obtained from Plasmix pyrolysis and Plasmix hydrogasification, including their corresponding peak areas and relative peak areas.

Author Contributions: Conceptualization, M.B.F. and L.D.P.; methodology, M.B.F. and L.D.P.; validation, M.B.F. and L.D.P.; investigation, M.B.F., S.T., L.D.P. and P.C.; data curation, M.B.F., S.T., L.D.P. and P.C.; writing—original draft preparation, M.B.F. and L.D.P.; writing—review and editing, G.C., P.C., F.C.L., G.M., A.G. and V.P.; visualization, M.B.F. and L.D.P.; supervision, A.G. and V.P.; funding acquisition, A.G. All authors have read and agreed to the published version of the manuscript.

Funding: This research was funded by Italian Ministry of Environment and Energy Security: I83C22001170006; Ministry of Universities and Research: I53C22001450006.

Institutional Review Board Statement: The study did not require ethical approval.

Informed Consent Statement: Not applicable.

Data Availability Statement: The original contributions presented in this study are included in the article/Supplementary Material. Further inquiries can be directed to the corresponding author.

Acknowledgments: This research was funded by the European Union—NextGenerationEU from the Italian Ministry of Environment and Energy Security, POR H2 AdP MEES/ENEA with involvement of CNR and RSE, PNRR—Mission 2, Component 2, Investment 3.5 "Ricerca e sviluppo sull'idrogeno", CUP: I83C22001170006. The authors also acknowledge Elisabetta Borsella (ENEA) for the GC-MS analysis. During the preparation of this manuscript/study, the authors used ChatGPT (OpenAI, GPT-6) to support language refinement, improve the clarity and readability of the manuscript, and enhance the visual quality of an existing figure without altering the presented scientific information. The authors have reviewed and edited the output and take full responsibility for the content of this publication.

Conflicts of Interest: The authors declare no conflicts of interest.

References

1. Mele, M.; Gurrieri, A.R.; Morelli, G.; Magazzino, C. Nature and Climate Change Effects on Economic Growth: An LSTM Experiment on Renewable Energy Resources. *Environ. Sci. Pollut. Res.* **2021**, *28*, 41127–41134. [CrossRef]
2. Chen, Y.; Chen, Y.; Zhang, L.; Li, Z. Revealing the Role of Renewable Energy Consumption and Digitalization in Energy-Related Greenhouse Gas Emissions—Evidence from the G7. *Front. Energy Res.* **2023**, *11*, 1197030. [CrossRef]
3. Yangin-Gomec, C.; Sárvári Horváth, I.; Martín, C. Energy Production from Biomass Valorization. *Energies* **2023**, *16*, 4300. [CrossRef]
4. Plastics Europe. *The Circular Economy for Plastics—A European Analysis 2024*; Plastics Europe: Brussels, Belgium, 2024.
5. Jiang, J.; Shi, K.; Zhang, X.; Yu, K.; Zhang, H.; He, J.; Ju, Y.; Liu, J. From Plastic Waste to Wealth Using Chemical Recycling: A Review. *J. Environ. Chem. Eng.* **2022**, *10*, 106867. [CrossRef]
6. Qureshi, M.S.; Oasmaa, A.; Pihkola, H.; Deviatkin, I.; Tenhunen, A.; Mannila, J.; Minkkinen, H.; Pohjakallio, M.; Laine-Ylijoki, J. Pyrolysis of Plastic Waste: Opportunities and Challenges. *J. Anal. Appl. Pyrolysis* **2020**, *152*, 104804. [CrossRef]
7. Cossu, R.; Garbo, F.; Girotto, F.; Simion, F.; Pivato, A. PLASMIX Management: LCA of Six Possible Scenarios. *Waste Manag.* **2017**, *69*, 567–576. [CrossRef]
8. Gazzotti, S.; De Felice, B.; Ortenzi, M.A.; Parolini, M. Approaches for Management and Valorization of Non-Homogeneous, Non-Recyclable Plastic Waste. *Int. J. Environ. Res. Public Health* **2022**, *19*, 10088. [CrossRef]
9. Ragaert, K.; Delva, L.; Van Geem, K. Mechanical and Chemical Recycling of Solid Plastic Waste. *Waste Manag.* **2017**, *69*, 24–58. [CrossRef]
10. Saraceno, E.; Ruocco, C.; Palma, V. A Review of Coal and Biomass Hydrogasification: Process Layouts, Hydrogasifiers, and Catalysts. *Catalysts* **2023**, *13*, 417. [CrossRef]
11. Gil, S.; Bialik, W.; Mocek, P.; Rimár, M.; Kizek, J.; Polivka, N. Investigation of the Kinetics of Pressure Coal Char Hydrogasification. *Energies* **2023**, *16*, 4937. [CrossRef]
12. Ha, D.T.; Tong, H.D.; Trinh, T.T. Insights into Hydro Thermal Gasification Process of Microplastic Polyethylene via Reactive Molecular Dynamics Simulations. *Sci. Rep.* **2024**, *14*, 18771. [CrossRef]
13. Liu, X.; Zheng, Y.; Liu, Z.; Ding, H.; Huang, X.; Zheng, C. Study on the Evolution of the Char Structure during Hydrogasification Process Using Raman Spectroscopy. *Fuel* **2015**, *157*, 97–106. [CrossRef]
14. Ding, X.; Zhang, Y.; Zhang, T.; Tang, J.; Xu, Y.; Zhang, J. Effect of Operational Variables on the Hydrogasification of Inner Mongolian Lignite Semicoke. *Energy Fuels* **2013**, *27*, 4589–4597. [CrossRef]
15. Tosti, S.; Spazzafumo, G.; Capobianco, D.; Buceti, G.; Pozio, A.; Bartucca, S. EU Scenarios of Renewable Coal Hydro-Gasification for SNG Production. *Sustain. Energy Technol. Assess.* **2016**, *16*, 43–52. [CrossRef]
16. Truong, T.B.T.; Ha, D.T.; Tong, H.D.; Trinh, T.T. Molecular Investigation of Pyrolysis and Thermal Gasification Pathways in Polyethylene Microplastics Degradation. *Chem. Eng. Process. Process Intensif.* **2025**, *213*, 110285. [CrossRef]
17. Saraceno, E.; Meloni, E.; Giaconia, A.; Palma, V. Catalytic OBSiC Open Cell Foams for Methane-Rich Gas Production through Hydrogasification of Plastic Waste. *Catalysts* **2025**, *15*, 152. [CrossRef]

18. Yan, L.; He, B.; Pei, X.; Wang, C.; Li, X.; Duan, Z. Kinetic Models for Coal Hydrogasification and Analyses of Hydrogasification Characteristics in Entrained-Flow Gasifiers. *Energy Fuels* **2013**, *27*, 6388–6396. [CrossRef]
19. Tosti, S.; Sousa, M.A.; Buceti, G.; Madeira, L.M.; Pozio, A. Process Analysis of Refuse Derived Fuel Hydrogasification for Producing SNG. *Int. J. Hydrogen Energy* **2019**, *44*, 21470–21480. [CrossRef]
20. Giaconia, A.; Tosti, S.; Caputo, G.; Pozio, A. Combustibili "Green" da Rifiuti ed Energie Rinnovabili. *La Chim. E l'Industria* **2022**, *104*, 52–57. [CrossRef]
21. *DIN 19539:2016-12*; Investigation of Solids–Temperature-Dependent Differentiation of Total Carbon (TOC_{400}, ROC, TIC_{900}). DIN Deutsches Institut für Normung: Berlin, Germany, 2016.
22. Channiwala, S.A.; Parikh, P.P. A Unified Correlation for Estimating HHV of Solid, Liquid and Gaseous Fuels. *Fuel* **2002**, *81*, 1051–1063. [CrossRef]
23. Alves, J.L.F.; Da Silva, J.C.G.; Da Silva Filho, V.F.; Alves, R.F.; Ahmad, M.S.; Ahmad, M.S.; Galdino, W.V.A.; De Sena, R.F. Bioenergy Potential of Red Macroalgae Gelidium floridanum by Pyrolysis: Evaluation of Kinetic Triplet and Thermodynamics Parameters. *Bioresour. Technol.* **2019**, *291*, 121892. [CrossRef]
24. Hayoune, F.; Chelouche, S.; Trache, D.; Zitouni, S.; Grohens, Y. Thermal Decomposition Kinetics and Lifetime Prediction of a PP/PLA Blend Supplemented with Iron Stearate during Artificial Aging. *Thermochim. Acta* **2020**, *690*, 178700. [CrossRef]
25. Kissinger, H.E. Reaction Kinetics in Differential Thermal Analysis. *Anal. Chem.* **1957**, *29*, 1702–1706. [CrossRef]
26. Li, K.Y.; Huang, X.; Fleischmann, C.; Rein, G.; Ji, J. Pyrolysis of Medium-Density Fiberboard: Optimized Search for Kinetics Scheme and Parameters via a Genetic Algorithm Driven by Kissinger's Method. *Energy Fuels* **2014**, *28*, 6130–6139. [CrossRef]
27. Cafiero, L.; Fabbri, D.; Trinca, E.; Tuffi, R.; Vecchio Ciprioti, S. Thermal and Spectroscopic (TG/DSC–FTIR) Characterization of Mixed Plastics for Materials and Energy Recovery under Pyrolytic Conditions. *J. Therm. Anal. Calorim.* **2015**, *121*, 1111–1119. [CrossRef]
28. Colantonio, S.; Cafiero, L.; De Angelis, D.; Ippolito, N.M.; Tuffi, R.; Vecchio Ciprioti, S. Thermal and Catalytic Pyrolysis of a Synthetic Mixture Representative of Packaging Plastics Residue. *Front. Chem. Sci. Eng.* **2020**, *14*, 288–303. [CrossRef]
29. Mumbach, G.D.; Alves, J.L.F.; Da Silva, J.C.G.; De Sena, R.F.; Marangoni, C.; Machado, R.A.F.; Bolzan, A. Thermal Investigation of Plastic Solid Waste Pyrolysis via the Deconvolution Technique Using the Asymmetric Double Sigmoidal Function: Determination of the Kinetic Triplet, Thermodynamic Parameters, Thermal Lifetime and Pyrolytic Oil Composition for Clean Energy Recovery. *Energy Convers. Manag.* **2019**, *200*, 112031. [CrossRef]
30. Cocchi, M.; De Angelis, D.; Mazzeo, L.; Nardozi, P.; Piemonte, V.; Tuffi, R.; Vecchio Ciprioti, S. Catalytic Pyrolysis of a Residual Plastic Waste Using Zeolites Produced by Coal Fly Ash. *Catalysts* **2020**, *10*, 1113. [CrossRef]
31. Cocchi, M.; Cafiero, L.; De Angelis, D.; Falasconi, M.B.; Piemonte, V.; Tuffi, R.; Vecchio Ciprioti, S. Conversion of Marine Plastic Litter into Chemicals and Fuels through Catalytic Pyrolysis Using Commercial and Coal Fly Ash-Synthesized Zeolites. *ACS Sustain. Chem. Eng.* **2023**, *11*, 3644–3656. [CrossRef]
32. Zolghadr, A.; Foroozandehfar, A.; Kulas, D.G.; Shonnard, D. Study of the Viscosity and Thermal Characteristics of Polyolefins/Solvent Mixtures: Applications for Plastic Pyrolysis. *ACS Omega* **2021**, *6*, 32832–32840. [CrossRef]
33. Zhang, M.; Hu, B.; Fan, G.; Yang, M.; Lu, Q.; Wu, Y. The Removal of Tar and the Production of Methane-Rich Gas from Biomass Hydrogen Pyrolysis by Using Biochar-Based Catalysts. *Energy Convers. Manag.* **2024**, *313*, 118596. [CrossRef]
34. Li, J.; Tian, Y.; Qiao, Y.; Chang, G.; Wang, C.; Gao, Y.; Yang, L.; Song, K.; Zhang, J.; Hu, S.; et al. Synergistic Effect of Hydrogen Atmosphere and Biochar Catalyst on Tar Decomposition and Methane-Rich Gas Production during Biomass Pyrolysis. *Fuel* **2022**, *330*, 125680. [CrossRef]
35. Al-Salem, S.M.; Lettieri, P.; Baeyens, J. Recycling and Recovery Routes of Plastic Solid Waste (PSW): A Review. *Waste Manag.* **2009**, *29*, 2625–2643. [CrossRef] [PubMed]
36. Tomita, A.; Mahajan, O.P.; Walker, P.L., Jr. Reactivity of Heat-Treated Coals in Hydrogen. *Fuel* **1977**, *56*, 137–144. [CrossRef]
37. Misirlioğlu, Z.; Canel, M.; Sinag, A. Hydrogasification of Chars under High Pressures. *Energy Convers. Manag.* **2007**, *48*, 52–58. [CrossRef]
38. Dao Thi, H.; Djokic, M.R.; Van Geem, K.M. Detailed Group-Type Characterization of Plastic-Waste Pyrolysis Oils: By Comprehensive Two-Dimensional Gas Chromatography Including Linear, Branched, and Di-Olefins. *Separations* **2021**, *8*, 103. [CrossRef]
39. Strien, J.R.J.; Genuino, H.C.; van Eijk, M.C.P.; Deuss, P.J.; Heeres, H.J. Pyrolysis of Polyolefin-Enriched Mixed Plastic Waste Streams: Effects of Pretreatments and Presence of Hydrogen during Pyrolysis. *Energy Fuels* **2025**, *39*, 686–698. [CrossRef]
40. Do, T.H.; Trinh, D.; Truong, T.B.T.; Trinh, T.T. Molecular Insights into Supercritical Water Gasification Process of Polyoxymethylene Plastics. *Sci. Rep.* **2025**, *15*, 9382. [CrossRef]

Disclaimer/Publisher's Note: The statements, opinions and data contained in all publications are solely those of the individual author(s) and contributor(s) and not of MDPI and/or the editor(s). MDPI and/or the editor(s) disclaim responsibility for any injury to people or property resulting from any ideas, methods, instructions or products referred to in the content.